Journal of Applied Physics

Picosecond ultrasonics for elasticity-based imaging and characterization of biological cells

Cite as: J. Appl. Phys. **128**, 160902 (2020); https://doi.org/10.1063/5.0023744
Submitted: 31 July 2020 . Accepted: 08 October 2020 . Published Online: 28 October 2020

Fernando Pérez-Cota, Rafael Fuentes-Domínguez, Salvatore La Cavera, William Hardiman, Mengting Yao, Kerry Setchfield, Emilia Moradi, Shakila Naznin, Amanda Wright, Kevin F. Webb, Alan Huett, Claire Friel, Virginie Sottile, Hany M. Elsheikha, Richard J. Smith, and Matt Clark

Journal of Applied Physics PERSPECTIVE scitation.org/journal/jap

Picosecond ultrasonics for elasticity-based imaging and characterization of biological cells

Cite as: J. Appl. Phys. **128**, 160902 (2020); doi: 10.1063/5.0023744
Submitted: 31 July 2020 · Accepted: 8 October 2020 ·
Published Online: 28 October 2020

Fernando Pérez-Cota,[1,a)] Rafael Fuentes-Domínguez,[1] Salvatore La Cavera,[1] William Hardiman,[1] Mengting Yao,[1] Kerry Setchfield,[1] Emilia Moradi,[1] Shakila Naznin,[1] Amanda Wright,[1] Kevin F. Webb,[1] Alan Huett,[2] Claire Friel,[2] Virginie Sottile,[3,4] Hany M. Elsheikha,[5] Richard J. Smith,[1] and Matt Clark[1]

AFFILIATIONS

[1]Optics and Photonics Group, Faculty of Engineering, University of Nottingham, Nottingham NG7 2RD, United Kingdom
[2]School of Life Sciences, University of Nottingham, Nottingham NG7 2RD, United Kingdom
[3]School of Medicine, University of Nottingham, Nottingham LE12 5RD, United Kingdom
[4]Department of Molecular Medicine, The University of Pavia, Pavia 27100, Italy
[5]School of Veterinary Medicine and Science, University of Nottingham, Sutton Bonington LE12 5RD, United Kingdom

Note: This paper is part of the Special Topic on Photothermics.
[a)]**Author to whom correspondence should be addressed:** fernando.perez-cota@nottingham.ac.uk

ABSTRACT

Characterization of the elasticity of biological cells is growing as a new way to gain insight into cell biology. Cell mechanics are related to most aspects of cellular behavior, and applications in research and medicine are broad. Current methods are often limited since they require physical contact or lack resolution. From the methods available for the characterization of elasticity, those relying on high frequency ultrasound (phonons) are the most promising because they offer label-free, high (even super-optical) resolution and compatibility with conventional optical microscopes. In this Perspective contribution, we review the state of the art of picosecond ultrasonics for cell imaging and characterization, particularly for Brillouin scattering-based methods, offering an opinion for the challenges faced by the technology. The challenges are separated into biocompatibility, acquisition speed, resolution, and data interpretation and are discussed in detail along with new results.

I. INTRODUCTION

A single biological cell holds the potential to copy itself trillions of times to create a macro-organism such as a human. Understanding this incredible capacity for transformation of matter and processing of energy is fundamental to understanding health[1–3] and developing biotechnologies.[4–6]

Many methods have been developed to study aspects of cells beyond that which is perceivable by an optical microscope.[7] Chemical, molecular, electrical, and mechanical structures are just some aspects that can be studied for which there are numerous technologies. As technology advances, it powers discovery improving the understanding of biology.

Cell mechanics (cytorheology) has historically remained largely unexplored compared to other aspects of cell biology. This is mainly because the available technologies have not advanced to a point at which they enable strong biological conclusions to be made. Most of the available technologies often require the application of physical stress to the cell, which can perturb the normal physiology through a variety of cell responses. In addition, the techniques often lack sufficient resolution, which limits characterization, capability particularly throughout the whole cell volume.

This lack of suitable technology and understanding of cell biomechanics is unsurprising given the difficulty of the problem: biological cells are very small, the parts that make them up exhibit little optical contrast, and they are extremely delicate when isolated. Attempting to measure the elastic properties as formally defined is difficult since the organization, shape, or orientation of sub-cellular components under the particular conditions in which a cell is

probed might influence the measured elastic parameters. Despite these challenges, practical demonstration of the characterization of the elasticity of cells has improved in recent times, generating interest, enabling practical applications and new discoveries.[8–13]

Among the new methods used to characterize the elasticity of cells, picosecond ultrasonics (PU)[14,15] is one of the most promising; combining the ability of conventional ultrasonics to resolve the time-of-flight of a coherent wavefront with the detection of sound-scattered light (Brillouin scattering).[16] This combination of features is unique and has enabled the first images of biological cells[17–20] using sub-optical wavelength ultrasound.

In this Perspective contribution, we address recent advances in PU for the characterization of cell elasticity. We provide our perspective on both the challenges and opportunities of the technology.

II. CHARACTERIZATION OF CELL ELASTICITY

Cell biomechanics can be defined as the mechanical attributes of cells and their substructures, along with their biological significance and influence on behavior. Cell biomechanics aims to increase our understanding of normal and disrupted cell physiology. Often, this involves studying the relationship of the elastic properties of a cell, with known biological functions. In recent years, single-cell biomechanics has become an area of growing interest. Differences in cell stiffness have been observed between cancer cells and normal cells, metastatic and benign cancer cells,[21–24] as well as other normal cellular processes. For instance, cell migration,[25] an essential process for immune cells and cancer metastasis, and mitotic division,[26] where cellular stiffness and cell–cell adhesion regulate mitotic rounding, a process critical for proliferation. Extracellular mechanical stimuli can also regulate cell processes such as the orientation axis during mitosis,[27] protein expression,[28] and cellular signaling through a process known as mechanotransduction.[29] This highlights the need to understand the mechanical properties of cells in response to their environment. It is known that the cytoskeleton serves as the underlying mechanical framework that enables cell normophysiology. The actin and tubulin cytoskeleton is conserved between all eukaryotes[30] (such as animals, fungi, plants, and algae), while prokaryotic cells (such as bacteria) have a cytoskeleton based on homologous filamentous proteins.[31] The fundamental mechanical difference between these cytoskeletons is poorly understood.

State of the art elasticity-characterization techniques can be roughly separated into two categories: contact and non-contact. Contact techniques include methods such as micropipette aspiration,[32,33] atomic force microscopy (AFM),[34–36] microfluidics,[37] and optical tweezers.[38–41] For all of these techniques, cells are placed under stress to observe a deformation, or the force required to achieve a set deformation is measured. Some of the effects of these deformation forces have been reported;[42] however, further understanding is needed.

Alternatively, non-contact methods use mechanical waves (sound) to probe the elasticity of cells. These methods are desirable as it is generally accepted that most cells do not exhibit disturbance by low power sound. For this reason, ultrasonic imaging remains the gold standard to image living human embryos *in utero*. Non-contact methods for the elastic characterization of cells include scanning acoustic microscopy (SAM),[43–45] Brillouin microscopy (BM),[46–48] photoacoustic microscopy (PAM),[49–51] and phonon microscopy (PM).[52] BM, PAM, and techniques based on PU currently achieve optical resolution; however, PU can provide a path for super-resolution.[53] Unlike BM, the probing frequency in PU is not optically limited, and the opto-acoustic nature of the interactions enables PU to overcome the limitations of piezoelectric transducers such as those used in SAM.

III. PICOSECOND ULTRASONICS

Picosecond ultrasonics (PU) was pioneered in the 1980s with the first generation and detection of coherent phonons. The breakthrough came with the ability to work in the GHz regime, which has been previously thought to be impossible. Ultrasonics in the GHz regime was achieved by the application of a novel variation of the pump–probe method using ultrashort laser pulses and a delay line.[14] A coherent phonon field was generated thermo-elastically and detected as variations in reflected intensity provided by the photoacoustic effect on a metallic thin film.[14,59] Soon after, the detection of Brillouin scattering as an interferometric signal was reported.[16] This form of Brillouin scattering is now commonly known as time-resolved Brillouin scattering (TRBS) and offered a way to obtain a measure of the sound velocity through a transparent and homogeneous medium.

These methods offer the opportunity to work at multi-GHz acoustic frequencies, which lead to the characterization at the bulk or thin-film scales of various materials. For instance, characterization of metallic thin films,[60,61] semiconductors,[62–64] dielectrics,[65–67] crystals,[68,69] or liquids.[55,70]

Another recent application of PU is characterization of the elastic properties of biological cells. Initially, this seemed an unlikely application: acquisition speed was low, substrates used were metallic films that generate heat, and the sample was simultaneously irradiated by both pump and probe beams (and often involving UV light). However, access to the Brillouin frequency shift (f_B) using TRBS is promising as it provides a measure of the sound velocity (v) at normal incidence,

$$f_B = 2nv/\lambda, \tag{1}$$

where n is the refractive index of the medium and λ is the optical probe wavelength. If the refractive index is known, then the sound velocity, an elastic property, could be mapped with optical resolution. This is a promising prospect since it enables non-contact characterization of biological cells with elasticity-related contrast and optical resolution—characteristics unavailable at the time by standard imaging techniques. The first report of TRBS from a biological cell came as single point measurements from an onion cell[71] approximately 20 years after the first report of detection of coherent phonons. Reports on mammalian cells[72] followed after, however, imaging remained challenging. Application of TRBS still posed several issues such as limited signal-to-noise ratio (SNR), low acquisition speed (only a few points per hour), and complex pump–probe system experimental arrangements. In these early systems, SNR could not be improved by simply increasing the

pump power or temporal averaging, as this typically leads to sample damage or motion artifacts.

The development of asynchronous optical sampling (ASOPS[73]) improved acquisition rates to a few points per second. An ASOPS pump–probe system uses two synchronized pulsed lasers, which operate at a slightly different repetition rate to provide a time-sweeping effect.[73] By removing the waiting time of the moving parts, the ASOPS systems reduced light exposure for the same SNR. This, in turn, enabled early high-quality images of biological cells using PU in fixed 3T3 fibroblast[17] and bone marrow[19] cells. However, living cells remained challenging until the development of cavity transducers for TRBS as well as the use of high thermal-conductivity substrates. These innovations enabled the first report on living cells[74] and the early insights into specific biological questions using TRBS.[52]

In addition to Brillouin scattering, PU also offers a GHz version of acoustic impedance imaging referred to as iPOM (inverted pulsed opto-acoustic microscope).[19] This method uses the reflection of a broadband (~100 GHz) acoustic pulse from a transducer-cell interface. In this way, it is possible to avoid damage from exposure to heat and light while remaining compatible with TRBS for extraction of quantitative elastic properties. This combined method allows the measurement of mass density and velocity properties close to the boundary of the transducer layer in a single instrument.[75] However, this has only been demonstrated for dehydrated cells, as the contrast mechanism requires a significant impedance mismatch between the cell and the surroundings, making it exceedingly difficult to apply to living cells.

The future of picosecond ultrasonics is promising. Elasticity based contrast has many applications in health and biology; resolution can be super-optical and the non-contact aspect of sound lends itself to label-free biocompatible operation. However, broad implementation of picosecond acoustics, and Brillouin scattering in particular, faces clear challenges that currently limit its applicability to those developing the technology. These include biocompatibility, signal-to-noise, acquisition speed, resolution, and data interpretation. In the context of biology, PU offers unique capabilities, which complement and extend other optical and elasticity-characterization techniques.

IV. PHONON MICROSCOPY: THE CHALLENGES

Our approach to PU is a novel form of TRBS that we call phonon microscopy[17,52,74] (see Fig. 1). In this method, the TRBS signal is collected in transmission through a custom designed opto-acoustic cavity transducer.[17] This configuration along with the use of an ASOPS laser configuration enabled a series of firsts: 3D reconstruction of the Brillouin frequency using cell phantoms,[17] live-cell imaging with sub-optical axial resolution,[74] and early investigations of specific biological questions.[76]

Figure 1(a) presents a simplified schematic of the phonon microscope. Two ASOPS[73] synchronized pulsed lasers (pump and probe, 390 and 780 nm, respectively) are delivered to the sample using an inverted microscope. The incident light is absorbed by an opto-acoustic transducer made from two gold layers separated by indium tin oxide (ITO).[17] The transmitted light, which carries the

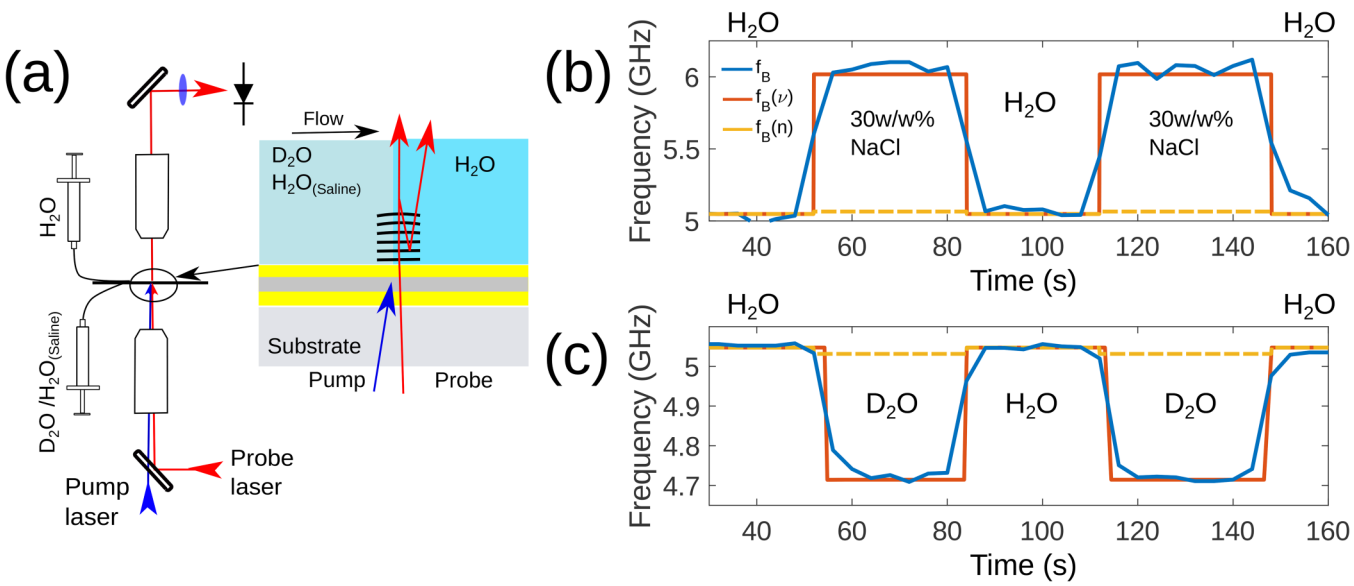

FIG. 1. Experimental setup and demonstration of sensitivity. (a) Experimental setup. (b) Brillouin frequency transition between water (H_2O) and 30 w/v% salt water. Variation of the sound velocity and refractive index between water[54,55] and 30 w/v% salt[56,57] is 20% and 0.4%, respectively. (c) Brillouin frequency transition between water and heavy water (D_2O). Variation of the sound velocity and refractive index between water and D_2O[54,58] is 7% and 0.3%, respectively. Dotted lines represent contribution of refractive index [$f_B(n)$ orange] and sound velocity [$f_B(v)$ red] individually to the Brillouin frequency f_B as estimated by theoretical approximations. In these cases, the sound velocity contributes at least 20 times more than the refractive index.

time-resolved signal, is collected by a second objective lens and directed to a photo-detector. The frequency of the detected signal is the Brillouin frequency, which is a direct measure of the sound velocity if the refractive index of the material under observation is known. Although the Brillouin frequency requires the knowledge of the refractive index, the contrast in an image depends on the relative weight of the velocity and refractive index variations in the sample; these determine whether the images are dominated by either its mechanical or optical properties.

Figure 1(b) demonstrates the sensitivity of f_B to the sound velocity. The change in f_B between water and 30 w/v% salt water was measured in a microfluidic channel. Laminar flow allowed fast switching between the two liquids. This removed any external influences leaving the variation of f_B exclusively due to the change in material properties. Since variations in sound velocity and refractive index are well characterized,[55–57,77] it is possible to estimate their individual contributions to f_B. These are included as dashed lines in yellow [$f_B(\nu)$ for refractive index] and solid red [$f_B(n)$ for sound velocity]. It is clear that the greater contribution, approximately 20 times larger, arises from the change in sound velocity—an elastic property. Furthermore, this is also visible if the two liquids have very small difference ($\sim 3 \times 10^{-3}$) in refractive index. For instance, Fig. 1(c) shows the change in f_B between water and heavy water where once again, sound velocity (ν) provides most of the contribution. These experiments demonstrate that, for a homogeneous liquid, ν dominates as the contrast mechanism when measuring f_B. This leads to qualitative elasticity characterization since the mass density remains unknown. Quantitative characterization based on ν depends on both density ρ and the longitudinal modulus M through the relation $\nu = \sqrt{M/\rho}$. In a complex biological material, the contribution of refractive index, density, and stiffness to the Brillouin frequency is a topic of ongoing discussion.[78–82]

Picosecond ultrasonics offers great prospects for the characterization of cell elasticity. In addition to the elasticity-related contrast, sound carries orders of magnitude less energy than photons of the same wavelength. This particular feature makes PU-based techniques non-invasive and live-cell compatible. This combination of characteristics remains possible for phonon wavelengths even shorter than those of visible light. This offers great promise for label-free, live-cell compatible super-resolution microscopy: a yet unavailable combination of capabilities in a single instrument. However, the technology is still in its infancy. There are a number of significant challenges that need to be addressed before this is possible. These include optimization of bio-compatibility, signal-to-noise ratio, lateral resolution, and interpretation of the data—each of which is discussed in detail in Secs. IV A–IV D.

A. Biocompatibility

Non-invasiveness is one of the promises of acoustic imaging as contrast is intrinsic and therefore does not require labels. As explained above, sound does not carry enough energy to cause molecular damage. Opto-acoustic detection methods using relatively long probing wavelengths (red to near infrared) minimize photodamage. However, for the particular case of picosecond ultrasonics, the situation is more challenging given that the specimen is attached to an opto-acoustic transducer (OAT) that generates heat as a by-product of generating sound and requires a relatively high-energy pump beam to make sound with sufficient amplitude to be measurable.

Phonon microscopy uses two lasers delivered through the same objective, which facilitates overlap of pump and probe spots (necessary to maximize signal) and reduces sample exposure to the probe light (single pass). However, maximizing transmittivity of the probe light causes leakage of the pump beam (390 nm), which limits biocompatibility to a few images per cell.[74] Alternative PU configurations have been reported[18,20] where the transducer is completely opaque to block all the pump light and the probe beam is delivered from the top. This removes exposure to pump light but causes two problems. (1) The overlap of the two tightly focused optical spots is challenging since the transducer is completely opaque so there is no optical reference for the position of both spots on a single camera. (2) The arrangement is more sensitive to environmental noise as the pump and probe spots originate from individual objectives.

To investigate the effect of phototoxicity of the pump and probe beams, cells were exposed to these beams while monitoring their health with propidium iodide (PI): a commonly used label that is excluded from healthy cells but generates a fluorescent signal on binding to DNA when the cell membrane has been compromised. In this case, the test was performed without an opto-acoustic transducer to prevent heat-induced damage. Figure 2 shows a test on fibroblast cells exposed to 390 nm pulsed laser light. Cell damage, visualized by the use of PI, is rapid at higher intensities [see Fig. 2(a)] and reduced at low doses [see Fig. 2(b)]. We estimated that only 5 mW · min (300 mJ, with $\lambda = 390$ nm, 150 fs pulses, 100 MHz repetition rate, and NA = 0.6) is required to kill a living 3T3 fibroblast cell. However, 40 mW/min (1.5 J) of 780 nm (dashed lines) did not cause any significant rise of the PI signal over longer timescales.

The next limit for biocompatibility is the temperature rise at the transducer/cell interface. In the previous work,[70] we demonstrated the ability of time-resolved Brillouin scattering to act as a temperature sensor. In the same work, the temperature rise of a single layer gold transducer at the tip of an optical fiber was measured to be 55 °C, which would be fatal to cells. In a cell imaging context, where power density is similar, it is possible to replace the glass substrate with materials that exhibit greater thermal conductivity.

Figure 3(a) shows a finite-element method (FEM) simulation of the steady-state average temperature rise in the imaging volume. The model considers average input power instead of the contributions of the individual pulses as this would be computationally unfeasible (100k+ pulses). Under typical experimental conditions,[17] the average temperature was estimated for three different substrates: glass, sapphire, and diamond. Glass exhibits a temperature rise which is incompatible with cell viability for practical average input powers (1–3 mW). For the same conditions, sapphire reduces the temperature rise to only 5 °C for 3 mW of input power while diamond practically removes any temperature rise. Experimental confirmation of the temperature rise at the transducer using sapphire and diamond substrates is also shown in Fig. 3(a)(*). Confirming the temperature rise when using glass substrates is a

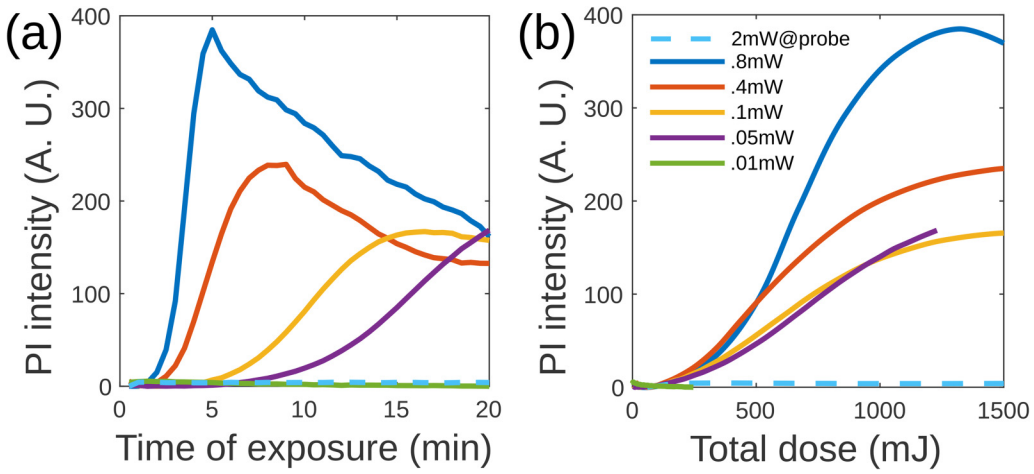

FIG. 2. Cell fluorescence from labeling with ambient propidium iodide (PI) upon exposure to pump and probe light. Intensity of PI against time (a) and total exposure (b) for different pump average powers. Dashed lines represent probe light and did not cause any visible rise in the PI signal for typical experimental conditions. In this case, there was no transducer to avoid heat-induced damage.

problem as the water approaches boiling temperature, introducing artifacts. While sapphire and diamond coverslips are expensive, they are much stronger than glass and can easily be reused.

Figure 3(b) shows a FEM simulation of the temperature profile in the transducer vicinity for the same cases as Fig. 3(a) using 1 mW input power for both beams combined. The maximum temperature rise occurs at the transducer and decays quickly within a few micrometers. Again, the temperature rise is high for glass, low for sapphire, and lowest for diamond. From these simulations, it is important to note that the maximum damage would occur at the contact points between the cell and the transducer, which could be alleviated by distancing the cell from the source of heat.

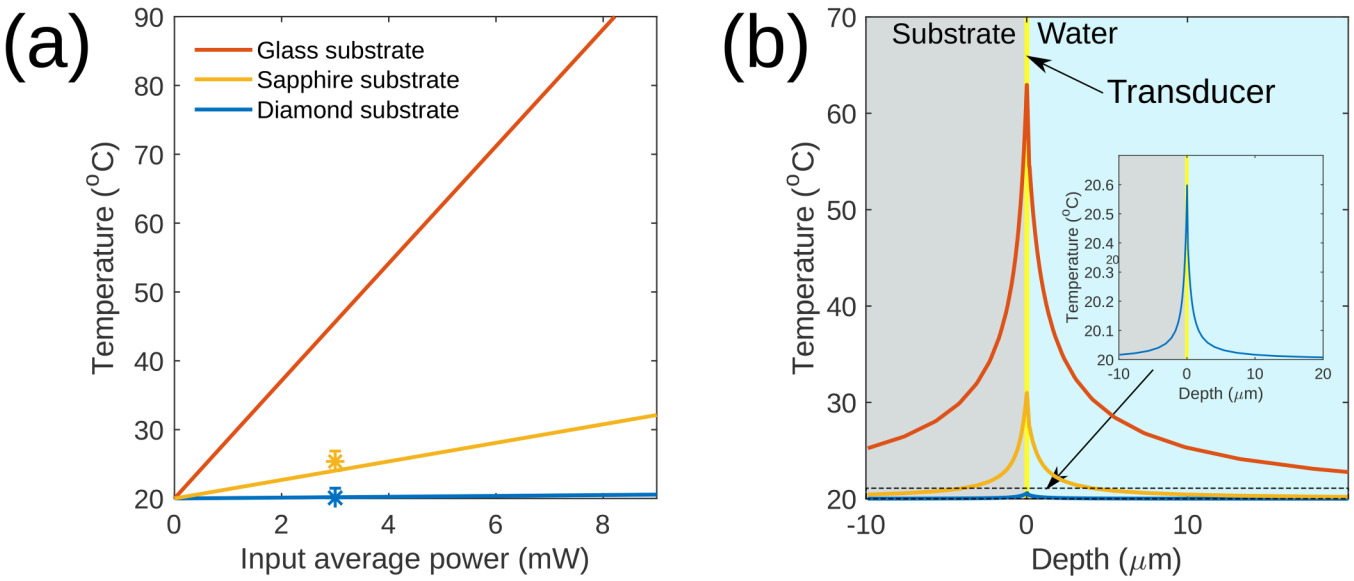

FIG. 3. Finite element method (FEM) simulation of temperature rise at the vicinity of the imaging spot. (a) Mean temperature rise against average input power for Au/ITO/Au cavity transducer in water using glass, sapphire, and diamond substrates. Solid lines represent calculation of the average temperature rise for the measured volume (∼cylinder with $r = 1\,\mu$m and $z = 10\,\mu$m) vs average power. The stars represent experimental measurements, where the temperature is estimated using the Brillouin frequency. (b) Temperature rise at the transducer vicinity for 3 mW input power. Temperature rise for diamond is below 1 °C at the transducer/water interface.

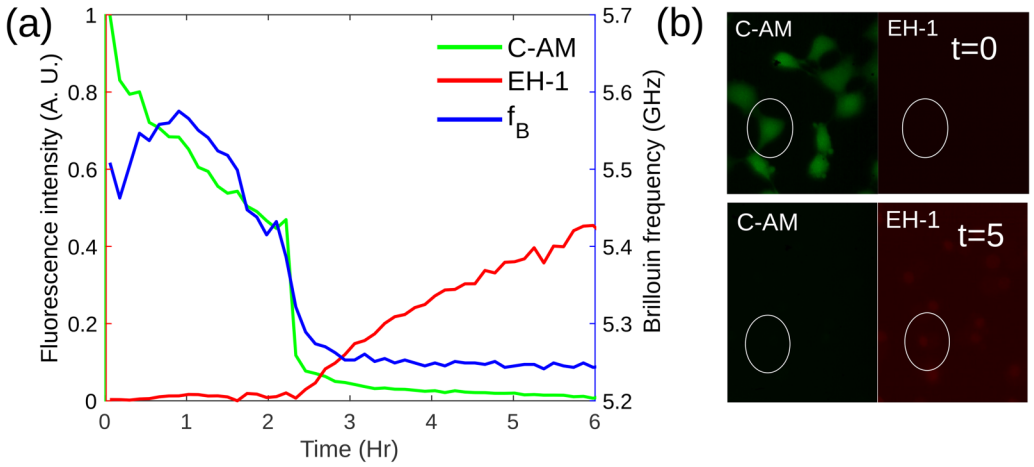

FIG. 4. Brillouin frequency f_B from live and dead cells. (a) Brillouin frequency and fluorescence live/dead assay (Calcein-AM/EH-1) of 3T3 fibroblast cells. (b) Example of live/dead fluorescence assay from the same cell at 0 and 5 h. The drop of Calcein-AM (C-AM) signal and the increase of ethidium homodimer-1 (EH-1) confirm cell death. The Brillouin frequency clearly correlates with the rise of C-AM signal and the fall of EH-1. The EH-1 has a similar function as PI while C-AM produces a fluorescence signal when the cell metabolism is active.

In terms of the elastic properties, normal and damaged cells differ (as shown in Fig. 4). These differences can be difficult to visualize optically; however, dead or damaged cells might not differ markedly from living cells in the short term. This is one of the reasons fluorescence based "live/dead" assays are the gold standard for establishing the health of cells *in vitro*. Although work with fixed cells is practical and can lead to useful insights, biocompatibility is crucial to enable live-cell imaging.

A configuration with near infrared (NIR) wavelengths for both pump and probe and high-thermal conductivity substrates would appear suitable for PU imaging of living cells, since at the expense of lateral resolution, it allows optical transparency without compromising biocompatibility. Both of these are key features that will enable wider incorporation of this technology. Figure 4(a) shows Brillouin frequency and fluorescence measured from cells before and after death using all-NIR wavelengths (780 nm for pump and probe) and sapphire coverslips. Cell death clearly affected the measured Brillouin frequency, which exhibited a sharp transition at the moment of death. This change might not be perceivable without the use of fluorescent labels. If biocompatibility is not considered, there is clear potential for the capture of unintended variations in the elastic properties of the specimens. Figure 4(b) shows the live/dead assay for the cells under study, which corroborates cell death approximately 2.5 h after the experiment started. The surrounding cells are also dead discarding the measurement process as the cause of death.

In summary, biocompatibility is important in any cell imaging context as it allows studying and following cell dynamics over time, while ensuring that responses and conditions are as close to normophysiological as possible. In the case of PU imaging, consideration and control of photon and thermal sources of damage need to be managed to achieve biocompatible operation. For this, the optimal selection of materials for the substrate and sound generation layers in conjunction with careful choice of optical wavelengths offers a viable way forward.

B. SNR and acquisition speed

Cell imaging using PU relies on the pump–probe method[16] to resolve the position and amplitude of phonon fields. Modulation depth of the detected signals is on the order of 10^{-4}–10^{-6}, which arise from weak light–sound interactions. Low modulation depth leads to averaging, which, in turn, increases the acquisition time linearly with the number of averages taken. Improving the signal-to-noise ratio (SNR) can thus result in either greater image quality or faster acquisition. The easiest way to increase modulation depth is by increasing the power of the pump beam; however, this generates a rise in temperature at the transducer and potential phototoxicity (see Sec. IV A).

Currently, there are two main transducer typologies: single layer[18,19,71] and three layer cavity-like transducers where the absorption is provided by either gold (Au)[17] or titanium (Ti).[20] It is hard to compare performance in terms of SNR of these typologies since not all reports communicate modulation depth, thermal rise, or the number of averages. However, to the best of our knowledge, our three-layer transducer is the only one that has produced images of living cells using TRBS.[17] To allow better comparisons, a different parameter is needed, one that reflects signal efficiency, e.g., the capability of the transducer to generate signal relative to the input power density.

Our transducer [see Fig. 1(a)] exhibits partial transparency at the probe wavelength and low transparency at the pump wavelength, which allows us to deliver both beams through the same objective in an inverted microscope configuration (signal is detected in transmission).[17] The transparency also allow us to perform brightfield imaging in transmission with good contrast.[17,74] This is a key feature as it facilitates finding the specimen and assessing its suitability for imaging. In contrast, Ti transducers are typically opaque and with high reflectivity. This is perhaps one reason why imaging dehydrated cells is often reported when using Ti transducers: a loss of contrast for bright-field imaging is experienced as the strong background reflection from the transducer

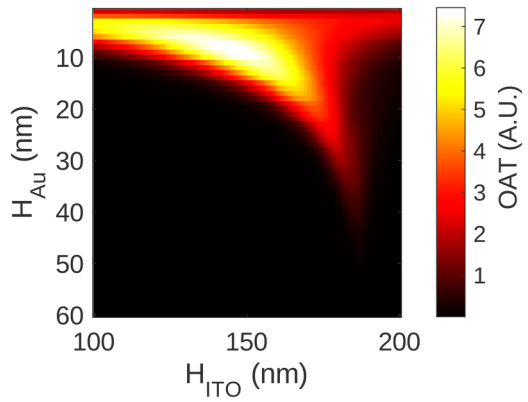

FIG. 5. Simulation of the performance for AU/ITO/Au cavity transducers for varying layer thicknesses. (a) The figure of merit for SNR per dose of pump light using UV (390 nm)/NIR (780 nm) wavelengths for pump and probe, respectively (OAT_{UV}). (b) The figure of merit using NIR wavelengths for both pump and probe (OAT_{NIR}). Fabrication tolerances are tight when considering the total dose of the pump beam; however, if an all-NIR (780 nm) configuration is used, tolerance to pump light increases that relaxes the fabrication tolerances significantly.

dominates the image of the cell. Consequently, it is hard to locate a specimen and assess its suitability for imaging.

We consider that the transducer and its substrate, in any given PU configuration, are the key to enhancing signal efficiency and managing thermal and photon loads. This, in turn, enables high SNR without compromising biocompatibility. The state of the art in transducer design is at an early stage, and there are many opportunities for improvement. Previously, we have designed our transducers for TRBS using separate optical and thermal-stress models.[17,83] However, a coupled optical-thermal-stress model[15] allows us to include the amplitude of the TRBS signal in the design of the transducer (see Fig. 5). Having a measure of transmittance at pump (T_{pump}), probe (T_{probe}), and relative Brillouin signal amplitude (A_{fB} in water), it is possible to produce a figure of merit (OAT) for our transducer performance using UV (390 nm) and NIR (780 nm) wavelengths for pump and probe, respectively,

$$OAT \propto \frac{A_{fB}{}^{*}SNR}{UV_{dose}}, \tag{2}$$

where $SNR \propto \sqrt{T_{probe}}$ and $UV_{dose} \propto T_{pump}/SNR^2$. The resultant figure of merit (OAT) shown in Fig. 5(a) indicates best performance at approximately dimensions of 10 nm and 150 nm for the Au and ITO layers, respectively. However, in practice, it is possible to increase the gold thickness to prevent UV leakage as much as possible. Our current transducer is a compromise between fabrication tolerances and biocompatibility: it blocks 90% of the pump light at a cost of signal SNR due to transmission efficiency (25%–30%).

In terms of temperature, cavity transducers also outperform single layers since most of the absorption occurs in the first layer (opposite the cell). As the spacing becomes greater, the temperature rise experienced by the specimen is reduced. We have estimated, through the finite element method (FEM), a steady-state thermal model. The model was used to calculate, for the same input power, the temperature rise from three transducers reported in the literature as shown in Fig. 6. A single Ti layer on sapphire[18] shows the greatest temperature rise at the sample. The Au/ITO/Au cavity on sapphire[17] has a manageable temperature rise and a spacing between layers of ~140 nm. The Ti/Si/Ti cavity[20] has small temperature rise due to a large spacing (10 μm) between the layers and the high thermal

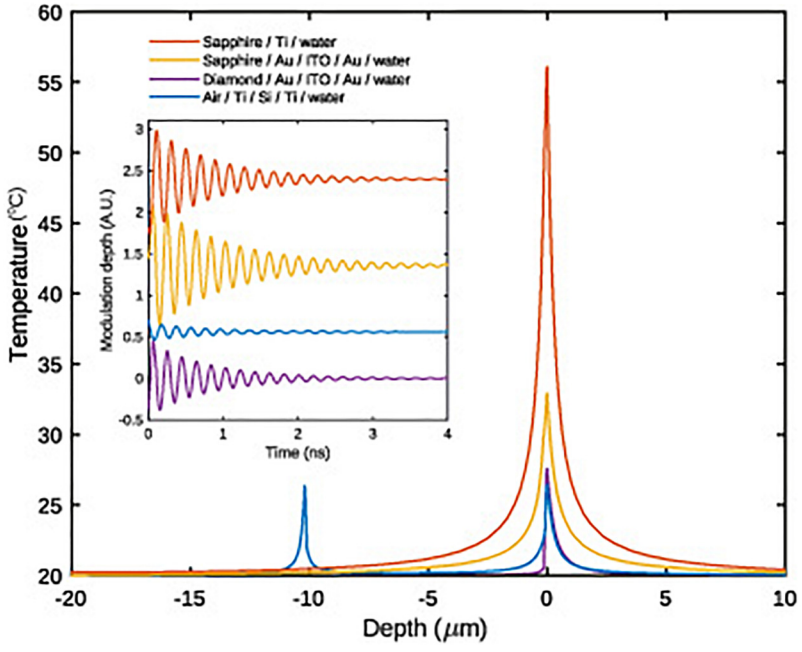

FIG. 6. Simulation of the thermal and acoustic performance of designs reported in the literature. Temperature rise for geometries of transducers made of a titanium layer on sapphire,[18] gold cavity on sapphire,[74]/diamond and a titanium cavity spaced by silicon.[20] The cell/transducer interface is located at depth = 0 μm. There is a clear difference between the configurations despite using the same input power being used for all cases. The best performance is provided by the substrates with higher thermal conductivity (silicon and diamond). The inset represents the acoustic response from water considering the same wavelengths and input powers, and it is apparent that the gold cavity has the strongest response. These simulations are an approximation but show the importance to optimize the transducer design.

conductivity of silicon. Finally, a gold cavity on diamond also shows only a small temperature rise due to highlighting the importance of the substrate in managing the temperature rise.

The generated signal amplitude for each transducer was also simulated through optical-thermal-stress model[15] to estimate the ability of each transducer to couple acoustic waves into a water medium. The inset in Fig. 6 suggests that our cavity transducer produces and couple waves with greater amplitude compared to competing architectures. For the case of the titanium cavity, the heat is spaced away from the cell (located at depth $= 0\,\mu$m). This spacing though brings significant attenuation of the phonon field, which is compensated by removing the substrate to direct more energy into the sample. Therefore, the Ti cavity[20] has no substrate in the area used for imaging: this allows practical signal amplitudes at low temperature and low power. However, the complexity of fabrication increases due to the need to etch a silicon wafer, the transducer remains opaque, and the area at which imaging can take place would have to remain small to retain structural integrity of the suspended transducer film.

Now the concept of limited acquisition speed will be addressed. This is central to the usability of PU in a practical setting and key to the future adoption of the technology. In pump–probe, the time resolution is given by the pulse length of the lasers, which allows bandwidth of up to a terahertz (if using femtosecond pulses). However, this ability comes with a compromise in the acquisition speed. The need for time reconstruction and averaging means that a 10 ns event takes millions of times longer to acquire.

There are several paths to improve this problem: enhancing signal amplitude so less averages are needed or using a parallel/wide-field method. Each one of these has the potential to improve the acquisition speed significantly, while carrying its own set of challenges. Enhancing signal amplitude requires increasing signal efficiency alongside managing thermally and photon induced damage (as discussed above). Parallel illumination aims to deliver simultaneously multiple points at the sample to increase the acquisition speed.[84] This gives rise to technical complexity and increased cost of instrumentation due to the need to deliver, align, and collect light from multiple tightly focused laser spots. High power lasers, additional conditioning optics, high well-depth cameras (due to low modulation depths), and multi-channel acquisition cards are required. Nevertheless, the acquisition speed might increase linearly with each additional measuring spot.

In summary, SNR and acquisition speed are key to enable broader use of the technology through the capacity to generate high quality images in short periods of time. Improving SNR can be achieved through the sophisticated transducer design; however, the acquisition speed remains a challenge as the timescales and volume of information are high. We expect future technological developments to offer alternatives on this front.

C. Phonon-based lateral resolution

Brillouin scattering is not the only available method for the detection of coherent phonon fields. Even though it offers a clear advantage in the form of simple detection that occurs at the wavefront rather than at a fixed position (i.e., transducer) and access to the sound velocity, it also has limitations. Most notably, the lateral resolution is set by the optics used and there is always the need to expose the sample to light. Aiming for acoustic wavelengths significantly smaller than of visible light is a limitation since wavelengths below 600 nm can easily induce photo-damage.[85]

We have reported the use of optically excited transducers for the generation of high quality factor, narrow band GHz ultrasound.[83] These can be used as generators and detectors and offer a way to set both the acoustic and optical wavelengths (see Fig. 7). Short acoustic wavelengths can enable greater-than-optical resolution, while the optical wavelengths can be set to optimize

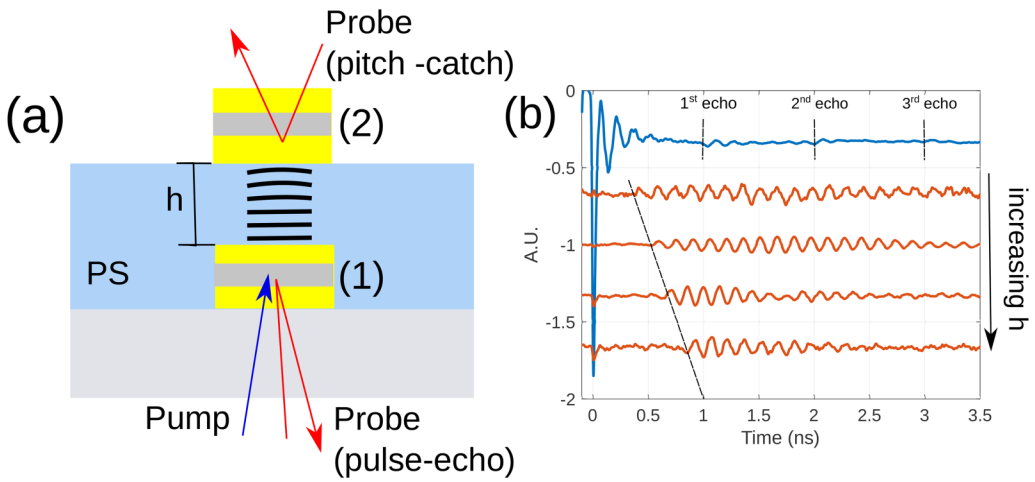

FIG. 7. Demonstration of opto-acoustic transducers as generators and detectors of GHz ultrasound. (a) Schematic setup. Two ultrasonic transducers are separated by a layer of polystyrene. The probe light path can be redirected for pulse-echo or pitch-catch detection. (b) Experimental GHz pulse echo (blue) and pitch-catch (red) detection of GHz ultrasound. The pulse-echo trace shows the initial excitation followed by three echoes. The pitch-catch traces come from different thicknesses of the PS layer, which increases the time of flight of the catch signal. Since the PS layer provides little damping, the transducer resonates with the arrival of the wave front.

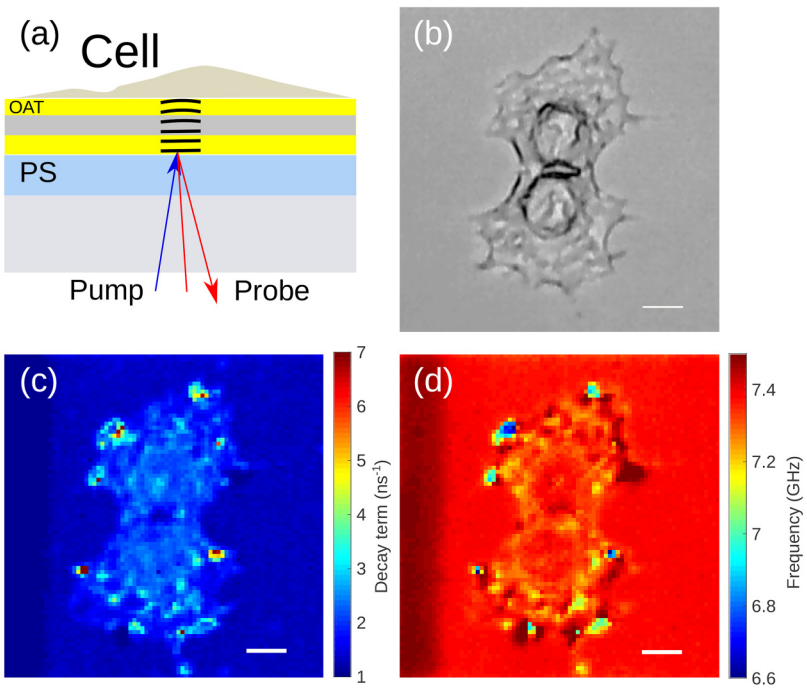

FIG. 8. Imaging a dehydrated cell using the acoustic damping of an ∼8 GHz transducer as a contrast mechanism. (a) Experimental setup. (b) Optical bright-field image. (c) Decay map. (d) Frequency map. The transducer is sensitive to the contact pressure of the material, which is a function of the properties and dimensions of the material in contact with it. This method is currently limited by optical diffraction but it can be expanded by exploiting the acoustical behaviors of opto-acoustic transducers. Scale bars are 5 μm.

absorption/reflection of the transducers. This can also solve biocompatibility problems removing the need for light to propagate through the cell at all.

Figure 7 shows a demonstration of generation and detection of GHz ultrasound. Two cavity transducers are separated by a polystyrene (PS) spacer layer of varying thicknesses between 1 and 2 μm. The transducers are made of a stack of two gold layers (Au, 30 nm) separated by indium tin oxide (ITO, 160 nm) with dimensions of $5 \times 5 \times 0.22\,\mu$m and operate at approximately 8 GHz. The experiment is set so that either transducer (1) serves as a generator and detector (pulse-echo) or transducer (1) serves as a generator and transducer (2) as a detector [pitch-catch, see Fig, 7(a)]. The blue trace in Fig. 7(b) represents pulse echo operation. At time zero, an excitation, which rapidly decays, is observed followed by three echoes. The red traces represent pitch catch operation for several PS thicknesses. As thickness increases, the time of flight of the wave packet also increases. Since the transducer is poorly damped by the soft PS spacer, it resonates causing a long oscillation.

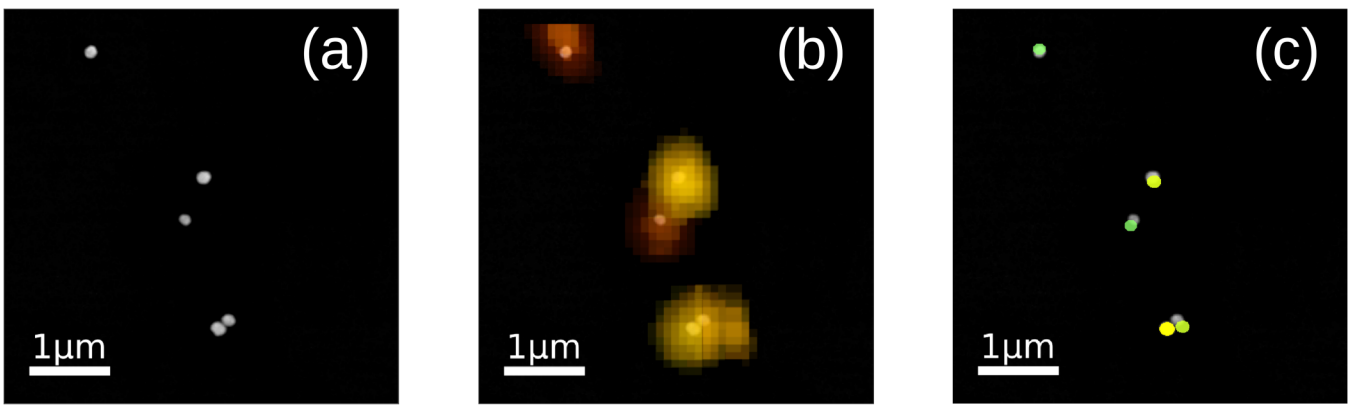

FIG. 9. Super-resolution imaging using nano-bells. Panel (a) is the scanning electron microscopy (SEM) image of a group of gold nanoparticles. Panel (b) is the overlay between the frequency given by the acoustic data and the SEM. Panel (c) is the reconstruction of the size and localization given by the acoustic data overlaid with the SEM, showing a very good agreement. This demonstrates the potential of sound to provide greater-than-optical resolution.

These simple experiments demonstrate that generation and detection of sub-optical wavelength ultrasound is possible. We plan to redesign these transducers to generate converging sound which can be focused to a volume below that achieved by an optical microscope. However, focusing a phonon field has its own difficulties. If a conventional acoustic lens design is considered, sound attenuation limits the maximum possible focal distance, which, in turn, limits the diameter of the lens. If the diameter of the lens is comparable in size with the acoustic wavelength, the focus will be poor and affected by artifacts. The scanning acoustic microscope faced these problems,[86,87] but we expect that the opto-acoustic nature of PU offers broader possibilities of design.

The transducers shown in Fig. 7 can also serve for acoustic impedance imaging[88,89] similar to iPOM. Since the transducer exhibits high quality factor, its resonance frequency and amplitude become sensitive to loading.[83] This approach differs to iPOM in that we trade the ability to sense different depths and resolutions (via broadband operation, ∼100 GHz) for sensitivity by operating in a narrow acoustic band (∼2 GHz). Figure 8 shows an example of cell imaging using its interaction from a narrow band transducer. A cell is grown on a transducer (non-patterned), and then dehydrated, and the transducer (from the opposite side to the cell) is scanned to build an image. The resulting images are produced from the following characteristics. Figure 8(c) shows the resonance frequency of the transducer: a measure of the mass loading (depending on density and volume) caused by the cell. Figure 8(d) shows the decay of the resonance: a measure of the impedance mismatch and the adherence of the cell to the substrate. A limitation of acoustic-impedance imaging is that its penetration depth is a function of the acoustic wavelength and typically low.

Acoustic impedance imaging, however, could be employed at a smaller scale. We anticipate that with the use of nano-patterning (such as electron beam lithography), it will be possible to confine the measurement to less than that can be optically resolved. In the past, we have demonstrated the ability of acoustics to identify nanoparticles within a single point spread function (PSF) by observing their acoustic signatures in a method we called nano-bells.[53] This concept could be applied for acoustic-impedance imaging such that the location and acoustic signature of each element on a grid will produce super-resolution acoustic images.

We also anticipate the use of nano-bells as acoustic "labels." Although this does require introducing the nanoparticles to the sample and is thus mildly invasive, acoustic labels offer great prospects: nanoparticles do not bleach, and their acoustic response is sensitive to the surrounding medium. Figure 9 shows the reconstruction of a group of five nanoparticles using PU. In Fig. 9(a), an electron microscopy image shows the nanoparticles grouped closely together so it would not be possible to resolve them optically. Figure 9(b) shows an opto-acoustic image where the color variation is related to frequency variation: acoustics can detect more than one acoustic signature in a single point spread function (PSF). Using the frequency and the centroid of each acoustic frequency, it is possible to identify the diameter and location of each particle resulting in the reconstruction shown in Fig. 9(c). The overlay with Fig. 9(a) is remarkably accurate when comparing with the electron micrograph. Nano-bells or nanoparticles as acoustic labels face their own set of challenges. The plasmonic particles used so far are relatively large (∼100 nm) and variation of particle radius as means of acoustic separation lends to an even greater increase in size. We expect that other particle types such as rods or disks[90] can offer a practical alternative due to rich spectral content. Nanoparticles also generate heat when optically excited; however, it might be possible to excite the particles with an external source of ultrasound.

In summary, resolution is one of the most important parameters of a microscope which is often obtained at the expense of biocompatibility. This is most obvious for electron microscopy[91] and super resolution techniques such as stimulation emission depletion (STED)[92] or stochastic optical reconstruction microscopy (STORM).[93] In this context, PU offers a unique opportunity through the use of coherent phonon fields, which we expect to be

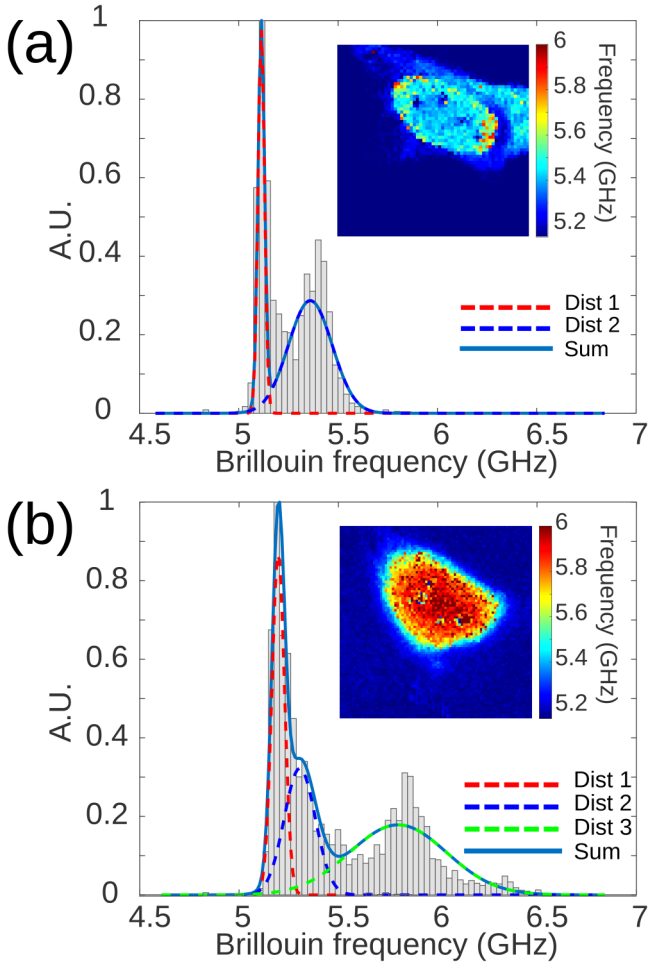

FIG. 10. Example of elastic responses of nocodazole-treated, formalin-fixed HeLa cells. (a) Brillouin spectra of a control HeLa cell. (b) Brillouin spectra of a Hela cell after administration of 0.1 ng/ml of nacodazole. Two and three distributions of f_B are observed in the spectra. Distribution 1 (red) corresponds to the surrounding medium. Distributions 2 (blue) and 3 (green) correspond to the cell and are different.

fully exploited in the future to obtain novel, mechanical information at resolutions that exceed those available using optics alone.

D. Data interpretation

Mechanics are relevant to many aspects of cell behavior, for instance, processes such as differentiation, migration, adhesion, division, or metastasis. Since elasticity is just starting to be explored at the cellular and sub-cellular scales, elasticity-based bio-markers are a possibility for aspects of biology such as lineage, pathology, or senescence. These and other aspects of cell biology offer vast possibilities for new discoveries in human, animal, or plant biology. However, discovery does not come automatically from strong sensitivity to the sound velocity. Interpretation of the results is

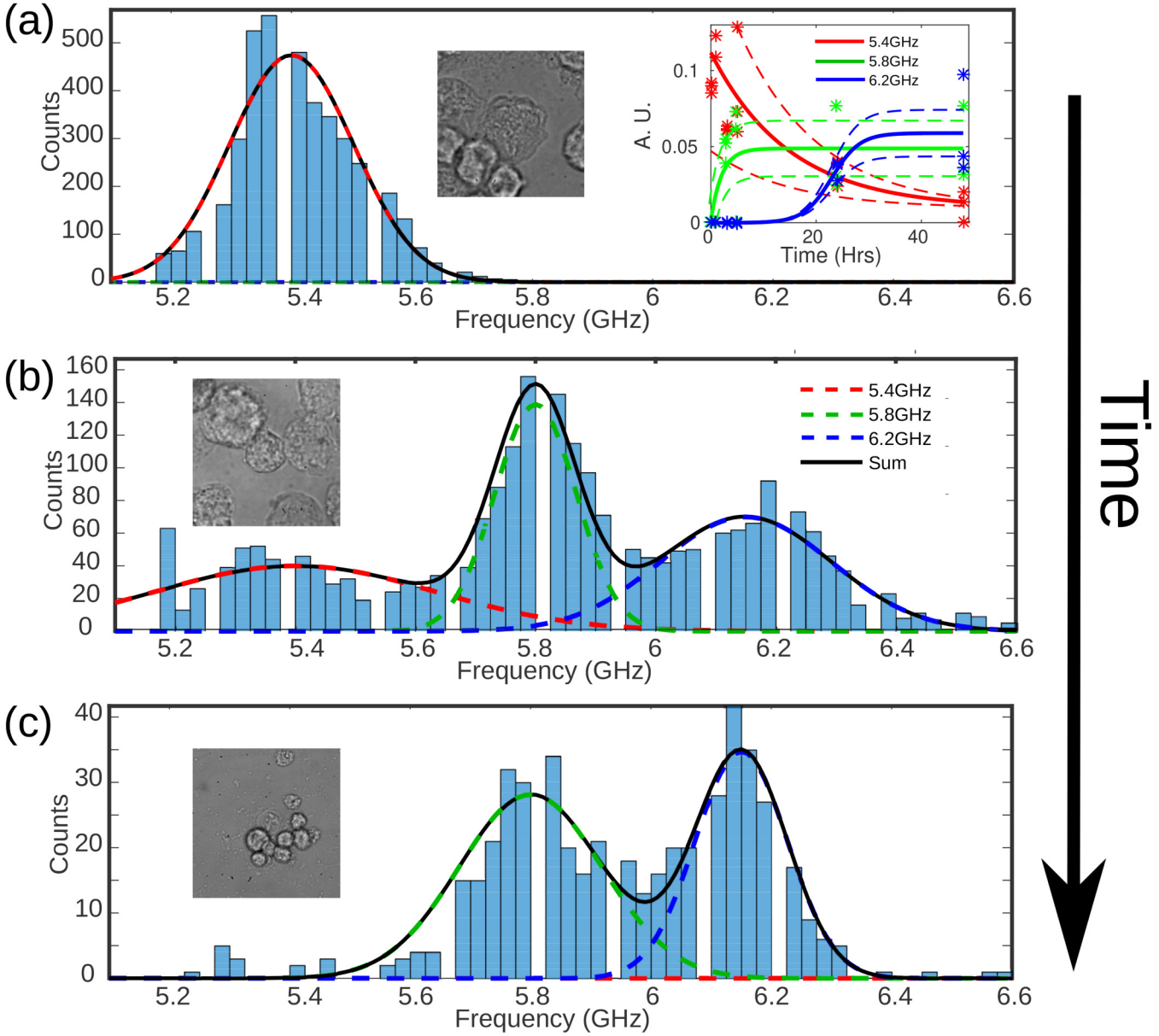

FIG. 11. Time series of the Brillouin spectrum of encysting *A. castellanii*.[52] Three frequency distributions are observed at 5.4, 5.8, and 6.2 GHz. The relative amplitude of the distributions changes with time. Brillouin spectrum at 1, 3, and 24 h is shown as (a)–(c), respectively. Panel (d) shows fitting of the data where complex dynamics are revealed. The ability of the *A. castellanii* to synthesize cellulose (5.8 GHz) quickly makes resistant to biocides long before the encystation process (2–3 days) is complete.

challenging because the data are heavily embedded in the time-resolved signal. There is a lack of descriptive models of phantoms for comparison at the relevant length scales, and any quantitative values yielded have little meaning as stand-alone measurements without correlation to other parameters of interest. Some of these problems will improve as more data are generated; however, during this period of technical expansion, it is important to explore many tools for the interpretation and application of the data.

For instance, we have exploited a wealth of knowledge in pharmacology to explore the mechanical consequences of the use of drugs which are, in many cases, well understood. Figure 10 demonstrates the effect of nocodazole on HeLa cells. There is a clear variation in the Brillouin spectrum obtained from these cells. Since nacodazole inhibits microtubule polymerization, it can be reasonable to hypothesize that this cytoskeletal alteration has mechanical consequences. It is possible to use specific fluorescence labeling in parallel to investigate the presence of particular materials within the cell. For instance, in a previous study we observed the synthesis of cellulose from *Acanthamoeba castellanii* encystation (see Fig. 11[52]). In this study, the cellulose created a distinct frequency peak in the Brillouin spectrum as confirmed by fluorescence staining within the amoebal cyst as it formed. This leads to a biologically relevant conclusion on the role of cellulose in encystation and the difficulty in treating *A. castellanii* related infections.

Typically, only the Brillouin frequency is extracted from a time-resolved signal; however, the use of all available signal characteristics can lead to useful contrast. Figure 12 shows a cell where the different signal characteristics are used as contrast and each one enable slightly different interpretation. Figure 12(a) presents the Brillouin frequency map taken as the average frequency of the time-resolved signal. The Brillouin frequency is an indirect measure of the sound velocity and is the most common form of imaging with Brillouin scattering. Additionally, using wavelet analysis, it is possible to resolve the signal frequency as a function of time.[18,19,74] As time of flight indicates the location of the acoustic wavefront, it is possible to section the volume with resolution greater than that of the optical depth of focus [see Fig. 12(b)[74]]. If decay of the signal is observed instead, then a measure of the sound attenuation coefficient (α_0) can be extracted.[76] Since sound can attenuate through scattering and absorption, α_0 is not a pure elastic property; however, it provides an alternative contrast mechanism which can be useful, for instance, to observe sub-nucleus structures [see Fig. 12(c)]. Another important aspect is the interaction of the cell with the substrate. By separating the initial amplitude from the effect of attenuation, it is possible to identify variations in the impedance mismatch with the substrate as well as potential areas of good and poor coupling. Figure 12(d) shows uniform coupling and little variation in amplitude between cytoplasm and medium; however, amplitude drops at the nucleus most likely due to impedance variations in crossing the multi-layered lipid structures.

These three signals characteristics (frequency, amplitude, and decay) are obvious choices to expand upon the possibilities of phonon imaging. However, it might be possible to find further characteristics. The origin of the signal is interferometric in nature, and the instantaneous phase might carry useful structural information that is not resolvable from the characteristics mentioned

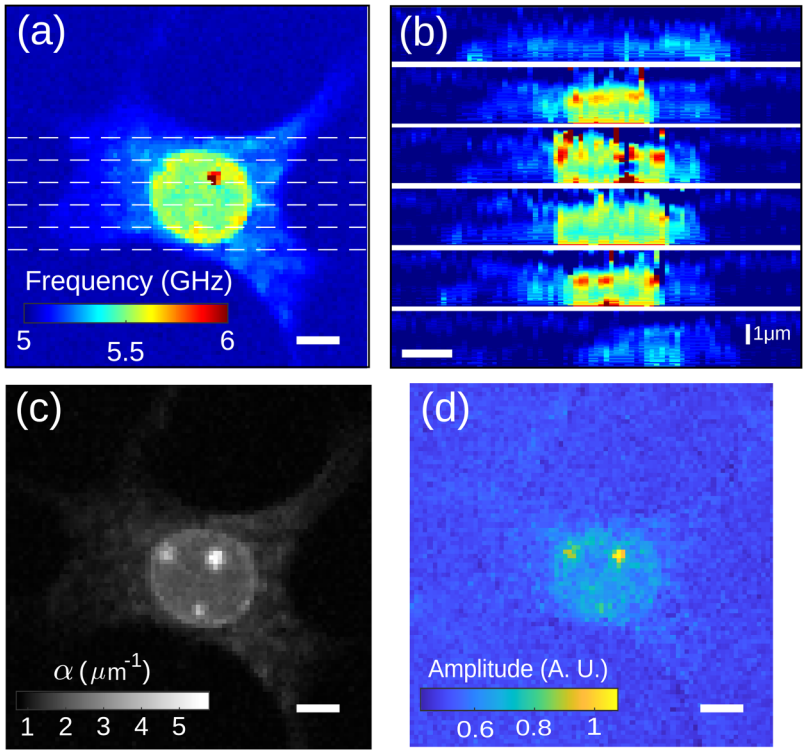

FIG. 12. Reconstruction of time-resolved data obtained from a 3T3 fibroblast cell. (a) Average frequency map. (b) XZ cross sections extracted from (a), as indicated by the dashed white lines, obtained using wavelet analysis in the time domain. (c) Map of the sound attenuation coefficient. (d) Map of the sound amplitude at t=0. Scale bar is 5 μm.

above. Deconvolving the signal to reconstruct the underlying structure from the time-resolved signal is challenging due to the occurrence of multiple reflections and noise. We expect that it will be possible to employ modern state of the art data mining methods[94–96] to enable interpretation of these instantaneous phase variations.

We are also exploring three key cell types with applications in healthcare and biology, which are challenging in terms of interpretation of the data. The first one, cardiac muscle cells [see Fig. 13(a)], is an intriguing cell type in terms of mechanics. Muscle cells contain a structure of fibers (sarcomeres), which are the functional unit of contraction. The striations ($\sim 2.2\,\mu$m) in the PU mechanical signal correspond to their periodicity, which are clearly visible in this image. Heart disease is one of the main causes of death in western countries, and the elastic behavior of cardiac cells might provide useful insights into both normophysiology and disease. Figure 13(b) shows a cell infected with *Toxoplasma gondii*: a cell-infecting parasite. As it invades the host cell, it forms a vacuole membrane from the membrane of the host cell rendering it resistant to the host immune system. As the parasite is compositionally different to the host cell, it generates significant contrast when imaging using a elasticity-related method. In terms of elasticity, the mechanics of infection and the influence of the parasite on the mechanics of the host cell are poorly understood. Finally, Fig. 13(c) shows a stem cell differentiating into an adipose cell. This type of cell has the ability to store energy in the body in the form of fat. Stem cells are responsible for healing the body and are the key to regenerative medicine. This is due to the fact that stem cells can transform to other cell types to replace damaged cells. Stem cell therapies are presently inhibited in their clinical translation, by the paucity of label-free biomarkers to confirm their state of differentiation, for fear of introducing harmful features, including tumorigenic mutations into patients. Differentiation as a process is poorly understood from a mechanical perspective. Here,

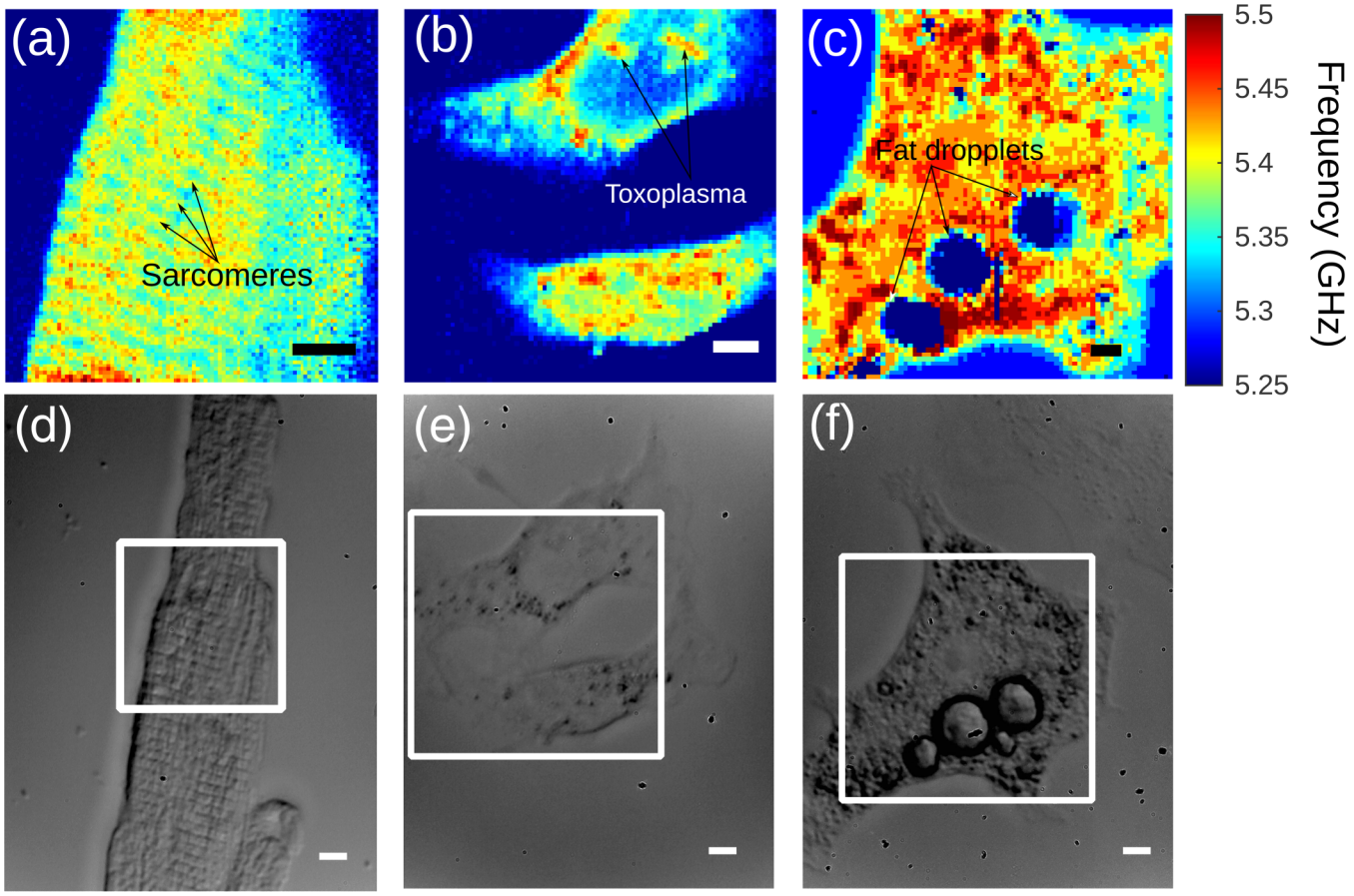

FIG. 13. Potential cell types for characterization of elasticity. (a) Cardiac muscle cells. The sarcomeres in these cells are the blocks that enable muscle contraction. (b) *Toxoplasma gondii*-infected cells. This single cell eukaryotic parasite causes mechanical stress to the cell membrane and cytoplasm. (c) Stem cells differentiating into adipose cells. The accumulation of fat by adipose cells is reflected by dramatic contrast in the Brillouin signature. (d)–(f) Bright-field images of cardiac, toxoplasma-infected, and adipose cells, respectively. Scale bar for all figures is 5 μm.

we demonstrate that elasticity offers intriguing prospects as the long-sought label-free differentiation biomarker since the differentiation of stem cells generates various mechanical features such as cytoskeletal remodeling, formation of fat droplets, or even sarcomeres.

In summary, it is clear that PU has the capability to enable discovery in various areas of biology. However, information within the time-resolved signal needs extraction and interpretation. In addition to improving technical capabilities, it is clear that a critical mass of experimental data and physical models are needed to realize the full potential of the technology.

V. SUMMARY

Cell mechanics and elasticity are fundamental aspects of biology. Novel elasticity-characterization tools are enabling discovery in many areas of biology and biomedical research where there are great opportunities to improve the technology and expand the areas of application. Picosecond ultrasonics offers a unique opportunity to enable elasticity-based, non-invasive, label-free super-resolution: a combination of features currently unavailable in a single instrument. The yet unsolved technological challenges preventing the consolidation of such capabilities are within the realm of engineering challenges, which we expect will be addressed in the near future.

AUTHORS' CONTRIBUTIONS

F.P.C., R.F.D., S.L.C., W.H., M.Y., K.F.W., R.J.S., and M.C. contributed to experiment design, simulations, practical work, and writing. K.S., E.M., and S.N. contributed to sample preparation. H.M.E., A.H., V.S., A.W., and C.F. contributed to application design. All authors edited the manuscript.

ACKNOWLEDGMENTS

Cardiac cells were kindly provided by Gil Bub and Rebecca Burton, Department of Physiology, Anatomy and Genetics, University of Oxford.

This work was supported by the Engineering and Physical Sciences Research Council (EPSRC) (Nos. EP/K021877/1 and EP/G061661/1), the Royal Academy of Engineering (RAEng) (No. RF20171817144), the RAEng/EPSRC Fellowship (No. EP/G058121/1), and the BBSRC (No. BB/K010212/1). V.S. was supported by a grant from the Italian Ministry of Education, University and Research (MIUR) to the Department of Molecular Medicine of the University of Pavia under the initiative "Dipartimenti di Eccellenza (2018–2022)."

DATA AVAILABILITY

The data that support the findings of this study are available from the corresponding author upon reasonable request.

REFERENCES

[1]X. Li, M. Dao, G. Lykotrafitis, and G. E. Karniadakis, "Biomechanics and biorheology of red blood cells in sickle cell anemia," J. Biomech. **50**, 34–41 (2017).
[2]C. P. Spatarelu, H. Zhang, D. T. Nguyen, X. Han, R. Liu, Q. Guo, J. Notbohm, J. Fan, L. Liu, and Z. Chen, "Biomechanics of collective cell migration in cancer progression: Experimental and computational methods," ACS Biomater. Sci. Eng. **5**, 3766–3787 (2019).
[3]D. Cox, C. Raeburn, X. Sui, and D. M. Hatters, "Protein aggregation in cell biology: An aggregomics perspective of health and disease," Semin. Cell. Dev. Biol. **99**, 40–54 (2020).
[4]M. Fröhling and M. Hiete, "Sustainability and life cycle assessment in industrial biotechnology: A review of current approaches and future needs," Adv. Biochem. Eng. Biotechnol. **173**, 143–203 (2020).
[5]L. Asveld, P. Osseweijer, and J. A. Posada, "Societal and ethical issues in industrial biotechnology," Adv. Biochem. Eng. Biotechnol. **173**, 121–141 (2020).
[6]A. Venkatesh, I. D. Posen, H. L. MacLean, P. L. Chu, W. M. Griffin, and B. A. Saville, "Environmental aspects of biotechnology," Adv. Biochem. Eng. Biotechnol. **173**, 77–119 (2020).
[7]A. R. Kherlopian, T. Song, Q. Duan, M. A. Neimark, M. J. Po, J. K. Gohagan, and A. F. Laine, "A review of imaging techniques for systems biology," BMC Syst. Biol. **2**, 74 (2008).
[8]A. Melhem and S. Conzen, "Connecting environmental stress to cancer cell biology through the neuroendocrine response," in *Encyclopedia of Environmental Health* (Elsevier, 2019), pp. 735–741.
[9]R. Alert and X. Trepat, "Physical models of collective cell migration," Annu. Rev. Condens. Matter Phys. **11**, 77–101 (2020).
[10]Y. L. Fan, H. C. Zhao, B. Li, Z. L. Zhao, and X. Q. Feng, "Mechanical roles of F-actin in the differentiation of stem cells: A review," ACS Biomater. Sci. Eng. **5**, 3788–3801 (2019).
[11]M. Li, D. Dang, L. Liu, N. Xi, and Y. Wang, "Atomic force microscopy in characterizing cell mechanics for biomedical applications: A review," IEEE Trans. NanoBiosci. **16**, 523–540 (2017).
[12]B. González-Bermúdez, G. V. Guinea, and G. R. Plaza, "Advances in micropipette aspiration: Applications in cell biomechanics, models, and extended studies," Biophys. J. **116**, 587–594 (2019).
[13]S. T. Spagnol, W. C. Lin, E. A. Booth, B. Ladoux, H. M. Lazarus, and K. N. Dahl, "Early passage dependence of mesenchymal stem cell mechanics influences cellular invasion and migration," Ann. Biomed. Eng. **44**, 2123–2131 (2016).
[14]C. Thomsen, J. Strait, Z. Vardeny, H. Maris, J. Tauc, and J. Hauser, "Coherent phonon generation and detection by picosecond light pulses," Phys. Rev. Lett. **53**, 989–992 (1984).
[15]O. Matsuda, M. C. Larciprete, R. Li Voti, and O. B. Wright, "Fundamentals of picosecond laser ultrasonics," Ultrasonics **56**, 3–20 (2015).
[16]C. Thomsen, H. Grahn, H. Maris, and J. Tauc, "Picosecond interferometric technique for study of phonons in the brillouin frequency range," Opt. Commun. **60**, 55–58 (1986).
[17]F. Pérez-Cota, R. J. Smith, E. Moradi, L. Marques, K. F. Webb, and M. Clark, "Thin-film optoacoustic transducers for subcellular brillouin oscillation imaging of individual biological cells," Appl. Opt. **54**, 8388 (2015).
[18]S. Danworaphong, M. Tomoda, Y. Matsumoto, O. Matsuda, T. Ohashi, H. Watanabe, M. Nagayama, K. Gohara, P. H. Otsuka, and O. B. Wright, "Three-dimensional imaging of biological cells with picosecond ultrasonics," Appl. Phys. Lett. **106**, 163701 (2015).
[19]T. Dehoux, M. Abi Ghanem, O. F. Zouani, J.-M. Rampnoux, Y. Guillet, S. Dilhaire, M.-C. Durrieu, and B. Audoin, "All-optical broadband ultrasonography of single cells," Sci. Rep. **5**, 8650 (2015).
[20]A. Viel, E. Péronne, O. Sénépart, L. Becerra, C. Legay, F. Semprez, L. Trichet, T. Coradin, A. Hamraoui, and L. Belliard, "Picosecond ultrasounds as elasticity probes in neuron-like cells models," Appl. Phys. Lett. **115**, 213701 (2019).
[21]S. E. Cross, Y. S. Jin, J. Rao, and J. K. Gimzewski, "Nanomechanical analysis of cells from cancer patients," Nat. Nanotechnol. **2**, 780–783 (2007).
[22]H. H. Lin, H. K. Lin, I. H. Lin, Y. W. Chiou, H. W. Chen, C. Y. Liu, H. I. Harn, W. T. Chiu, Y. K. Wang, M. R. Shen, and M. J. Tang, "Mechanical phenotype of cancer cells: Cell softening and loss of stiffness sensing," Oncotarget **6**, 20946–20958 (2015).
[23]M. Brandao, A. Fontes, M. Barjas-Castro, L. Barbosa, F. Costa, C. Cesar, and S. Saad, "Optical tweezers for measuring red blood cell elasticity: Application to

the study of drug response in sickle cell disease," Eur. J. Haematol. **70**, 207–211 (2003).
[24]S. Pelucchi, R. Stringhi, and E. Marcello, "Dendritic spines in Alzheimer's disease: How the actin cytoskeleton contributes to synaptic failure," Int. J. Mol. Sci. **21**, 908 (2020).
[25]F. Lautenschläger, S. Paschke, S. Schinkinger, A. Bruel, M. Beil, and J. Guck, "The regulatory role of cell mechanics for migration of differentiating myeloid cells," Proc. Natl. Acad. Sci. U.S.A. **106**, 15696–15701 (2009).
[26]A. Nematbakhsh, W. Sun, P. A. Brodskiy, A. Amiri, C. Narciso, Z. Xu, J. J. Zartman, and M. Alber, "Multi-scale computational study of the mechanical regulation of cell mitotic rounding in epithelia," PLoS Comput. Biol. **13**, e1005533 (2017).
[27]L. Zhao, C. Sang, C. Yang, and F. Zhuang, "Effects of stress fiber contractility on uniaxial stretch guiding mitosis orientation and stress fiber alignment," J. Biomech. **44**, 2388–2394 (2011).
[28]J. H. C. Wang and B. P. Thampatty, "An introductory review of cell mechanobiology," Biomech. Model. Mechanobiol. **5**, 1–16 (2006).
[29]A. W. Orr, B. P. Helmke, B. R. Blackman, and M. A. Schwartz, "Mechanisms of mechanotransduction," Dev. Cell. **10**, 11–20 (2006).
[30]J. Hardin, G. P. Bertoni, and L. J. Kleinsmith, *Becker's World of the Cell* (Pearson Higher Ed, 2017).
[31]H. P. Erickson, "The discovery of the prokaryotic cytoskeleton: 25th anniversary," Mol. Biol. Cell. **28**, 357–358 (2017).
[32]R. M. Hochmuth, "Micropipette aspiration of living cells," J. Biomech. **33**, 15–22 (2000).
[33]D. P. Theret, "Application of the micropipette technique to the measurement of cultured porcine aortic endothelial cell viscoelastic properties," J. Biomech. Eng. **112**, 263 (2008).
[34]Z. Shao, J. Yang, and A. P. Somlyo, "Biological atomic force microscopy: From microns to nanometers and beyond," Annu. Rev. Cell Dev. Biol. **11**, 241–65 (1995).
[35]M. Rief, "Reversible unfolding of individual titin immunoglobulin domains by AFM," Science **276**, 1109–1112 (1997).
[36]P. Parot, Y. F. Dufrêne, P. Hinterdorfer, C. Le Grimellec, D. Navajas, J.-L. Pellequer, and S. Scheuring, "Past, present and future of atomic force microscopy in life sciences and medicine," J. Mol. Recognit. **20**, 418–31 (2007).
[37]R. B. Morrish, M. Hermes, J. Metz, N. Stone, S. Pagliara, R. Chahwan, and F. Palombo, "Single cell imaging of nuclear architecture changes," Front. Cell Dev. Biol. **7**, 141 (2019).
[38]J. Sleep, D. Wilson, R. Simmons, and W. Gratzer, "Elasticity of the red cell membrane and its relation to hemolytic disorders: An optical tweezers study," Biophys. J. **77**, 3085–95 (1999).
[39]S. Hénon, G. Lenormand, A. Richert, and F. Gallet, "A new determination of the shear modulus of the human erythrocyte membrane using optical tweezers," Biophys. J. **76**, 1145–51 (1999).
[40]E. Fällman, S. Schedin, J. Jass, M. Andersson, B. E. Uhlin, and O. Axner, "Optical tweezers based force measurement system for quantitating binding interactions: System design and application for the study of bacterial adhesion," Biosens. Bioelectron. **19**, 1429–1437 (2004).
[41]H. Zhang and K.-K. Liu, "Optical tweezers for single cells," J. R. Soc. Interface **5**, 671–90 (2008).
[42]Y. Z. Yoon, J. Kotar, A. T. Brown, and P. Cicuta, "Red blood cell dynamics: From spontaneous fluctuations to non-linear response," Soft Matter **7**, 2042–2051 (2011).
[43]J. A. Hildebrand, D. Rugar, R. N. Johnston, and C. F. Quate, "Acoustic microscopy of living cells," Proc. Natl. Acad. Sci. U.S.A. **78**, 1656–60 (1981).
[44]T. Kundu, J. Bereiter-Hahn, and I. Karl, "Cell property determination from the acoustic microscope generated voltage versus frequency curves," Biophys. J. **78**, 2270–9 (2000).
[45]K. Miura and S. Yamamoto, "A scanning acoustic microscope discriminates cancer cells in fluid," Sci. Rep. **5**, 15243 (2015).
[46]G. Scarcelli, W. J. Polacheck, H. T. Nia, K. Patel, A. J. Grodzinsky, R. D. Kamm, and S. H. Yun, "Noncontact three-dimensional mapping of intracellular hydromechanical properties by Brillouin microscopy," Nat. Methods **12**, 1132–1134 (2015).
[47]K. Elsayad, S. Werner, M. Gallemí, J. Kong, E. R. Sánchez Guajardo, L. Zhang, Y. Jaillais, T. Greb, and Y. Belkhadir, "Mapping the subcellular mechanical properties of live cells in tissues with fluorescence emission-Brillouin imaging," Sci. Signaling **9**, rs5 (2016).
[48]G. Scarcelli, "Brillouin microscopy to image cell and tissue mechanical properties," in *Optics in the Life Sciences Congress* (OSA, Washington, DC, 2017), p. BoTu3A.1.
[49]C. Zhang, Y. S. Zhang, D.-K. Yao, Y. Xia, and L. V. Wang, "Label-free photoacoustic microscopy of cytochromes," J. Biomed. Opt. **18**, 20504 (2013).
[50]E. M. Strohm, M. J. Moore, and M. C. Kolios, "Single cell photoacoustic microscopy: A review," IEEE J. Sel. Top. Quantum Electron. **22**, 137–151 (2016).
[51]E. M. Strohm, M. J. Moore, and M. C. Kolios, "High resolution ultrasound and photoacoustic imaging of single cells," Photoacoustics **4**, 36–42 (2016).
[52]F. Pérez-Cota, R. J. Smith, H. M. Elsheikha, and M. Clark, "New insights into the mechanical properties of *Acanthamoeba castellanii* cysts as revealed by phonon microscopy," Biomed. Opt. Express **10**, 2399 (2019).
[53]R. Fuentes-Domínguez, F. Pérez-Cota, S. Naznin, R. J. Smith, and M. Clark, "Super-resolution imaging using nano-bells," Sci. Rep. **8**, 16373 (2018).
[54]S. Kedenburg, M. Vieweg, T. Gissibl, and H. Giessen, "Linear refractive index and absorption measurements of nonlinear optical liquids in the visible and near-infrared spectral region," Opt. Mater. Express **2**, 1588 (2012).
[55]F. Yang, T. J. Grimsley, S. Che, G. A. Antonelli, H. J. Maris, and A. V. Nurmikko, "Picosecond ultrasonic experiments with water and its application to the measurement of nanostructures," J. Appl. Phys. **107**, 103537 (2010).
[56]K. V. Mackenzie, "Discussion of sea water sound-speed determinations," J. Acoust. Soc. Am. **70**, 801–806 (1981).
[57]X. Quan and E. S. Fry, "Empirical equation for the index of refraction of seawater," Appl. Opt. **34**, 3477 (1995).
[58]R. Wegge, M. Richter, and R. Span, "Speed of sound measurements in deuterium oxide (D_2O) over the temperature range from (278.2 to 353.2) K at pressures up to 20 MPa," Fluid Phase Equilib. **418**, 175–180 (2016).
[59]C. Thomsen, H. Grahn, H. Maris, and J. Tauc, "Surface generation and detection of phonons by picosecond light pulses," Phys. Rev. B **34**, 4129–4138 (1986).
[60]G. L. Eesley, B. M. Clemens, and C. A. Paddock, "Generation and detection of picosecond acoustic pulses in thin metal films," Appl. Phys. Lett. **50**, 717 (1987).
[61]O. Matsuda and O. B. Wright, "Reflection and transmission of light in multilayers perturbed by picosecond strain pulse propagation," J. Opt. Soc. Am. B **19**, 3028 (2002).
[62]H. Ogi, T. Shagawa, N. Nakamura, M. Hirao, H. Odaka, and N. Kihara, "Elastic-constant measurement in oxide and semiconductor thin films by brillouin oscillations excited by picosecond ultrasound," Jpn. J. Appl. Phys. **48**, 07GA01 (2009).
[63]C. M. Hernandez, T. W. Murray, and S. Krishnaswamy, "Photoacoustic characterization of the mechanical properties of thin films," Appl. Phys. Lett. **80**, 691 (2002).
[64]P. Emery and A. Devos, "Acoustic attenuation measurements in transparent materials in the hypersonic range by picosecond ultrasonics," Appl. Phys. Lett. **89**, 191904 (2006).
[65]C. J. Morath and H. J. Maris, "Phonon attenuation in amorphous solids studied by picosecond ultrasonics," Phys. Rev. B **54**, 203–213 (1996).
[66]S. Ayrinhac, M. Foret, A. Devos, B. Rufflé, E. Courtens, and R. Vacher, "Subterahertz hypersound attenuation in silica glass studied via picosecond acoustics," Phys. Rev. B **83**, 014204 (2011).
[67]H. N. Lin, R. J. Stoner, H. J. Maris, and J. Tauc, "Phonon attenuation and velocity measurements in transparent materials by picosecond acoustic interferometry," J. Appl. Phys. **69**, 3816–3822 (1991).
[68]C. Rossignol, "Nondestructive evaluation of micrometric diamond films with an interferometric picosecond ultrasonics technique," J. Appl. Phys. **95**, 4157 (2004).

[69]D. Hurley, O. Wright, O. Matsuda, V. Gusev, and O. Kolosov, "Laser picosecond acoustics in isotropic and anisotropic materials," Ultrasonics **38**, 470–474 (2000).
[70]S. L. Cavera, F. Pérez-Cota, R. Fuentes-Domínguez, R. J. Smith, and M. Clark, "Time resolved brillouin fiber-spectrometer," Opt. Express **27**, 25064–25071 (2019).
[71]C. Rossignol, N. Chigarev, M. Ducousso, B. Audoin, G. Forget, F. Guillemot, and M. C. Durrieu, "In vitro picosecond ultrasonics in a single cell," Appl. Phys. Lett. **93**, 123901 (2008).
[72]M. Ducousso, O. El-Farouk Zouani, C. Chanseau, C. Chollet, C. Rossignol, B. Audoin, and M.-C. Durrieu, "Evaluation of mechanical properties of fixed bone cells with sub-micrometer thickness by picosecond ultrasonics," Eur. Phys. J. Appl. Phys. **61**, 11201 (2013).
[73]P. A. Elzinga, F. E. Lytle, Y. Jian, G. B. King, and N. M. Laurendeau, "Pump/probe spectroscopy by asynchronous optical sampling," Appl. Spectrosc. **41**, 2–4 (1987).
[74]F. Pérez-Cota, R. J. Smith, E. Moradi, L. Marques, K. F. Webb, and M. Clark, "High resolution 3D imaging of living cells with sub-optical wavelength phonons," Sci. Rep. **6**, 39326 (2016).
[75]L. Liu, L. Plawinski, M. Durrieu, and B. Audoin, "Label-free multi-parametric imaging of single cells: Dual picosecond optoacoustic microscopy," J. Biophotonics **12**, e201900045 (2019).
[76]F. Pérez-Cota, S. La Cavera, S. Naznin, R. Fuentes-Domínguez, R. J. Smith, and M. Clark, "Apparent attenuation by opto-acoustic defocus in phonon microscopy," Photoacoustics **19**, 100180 (2020).
[77]P. Schiebener, J. Straub, J. M. H. Levelt Sengers, and J. S. Gallagher, "Refractive index of water and steam as function of wavelength, temperature and density," J. Phys. Chem. Ref. Data **19**, 677 (1990).
[78]P.-J. Wu, I. V. Kabakova, J. W. Ruberti, J. M. Sherwood, I. E. Dunlop, C. Paterson, P. Török, and D. R. Overby, "Water content, not stiffness, dominates brillouin spectroscopy measurements in hydrated materials," Nat. Methods **15**, 561–562 (2018).
[79]G. Scarcelli and S. H. Yun, "Reply to 'Water content, not stiffness, dominates Brillouin spectroscopy measurements in hydrated materials'," Nat. Methods **15**, 562–563 (2018).
[80]M. Bailey, M. Alunni-Cardinali, N. Correa, S. Caponi, T. Holsgrove, H. Barr, N. Stone, C. P. Winlove, D. Fioretto, and F. Palombo, "Brillouin-derived viscoelastic parameters of hydrogel tissue models," Sci. Adv. (in press) (2020).
[81]G. Antonacci, T. Beck, A. Bilenca, J. Czarske, K. Elsayad, J. Guck, K. Kim, B. Krug, F. Palombo, R. Prevedel, and G. Scarcelli, "Recent progress and current opinions in Brillouin microscopy for life science applications," Biophys. Rev. **12**, 615–624 (2020).
[82]J. Margueritat, A. Virgone-Carlotta, S. Monnier, H. Delanoë-Ayari, H. C. Mertani, A. Berthelot, Q. Martinet, X. Dagany, C. Rivière, J.-P. Rieu, and T. Dehoux, "High-frequency mechanical properties of tumors measured by Brillouin light scattering," Phys. Rev. Lett. **122**, 018101 (2019).
[83]R. J. Smith, F. P. Cota, L. Marques, X. Chen, A. Arca, K. Webb, J. Aylott, M. G. Somekh, and M. Clark, "Optically excited nanoscale ultrasonic transducers," J. Acoust. Soc. Am. **137**, 219–227 (2015).
[84]R. J. Smith, R. A. Light, S. D. Sharples, N. S. Johnston, M. C. Pitter, and M. G. Somekh, "Multichannel, time-resolved picosecond laser ultrasound imaging and spectroscopy with custom complementary metal-oxide-semiconductor detector," Rev. Sci. Instrum. **81**, 024901 (2010).
[85]M. Nikolić and G. Scarcelli, "Long-term Brillouin imaging of live cells with reduced absorption-mediated damage at 660 nm wavelength," Biomed. Opt. Express **10**, 1567 (2019).
[86]V. Jipson and C. F. Quate, "Acoustic microscopy at optical wavelengths," Appl. Phys. Lett. **32**, 789–791 (1978).
[87]B. Hadimioglu, "Water acoustic microscopy at suboptical wavelengths," Appl. Phys. Lett. **43**, 1006 (1983).
[88]M. N. Fadhel, E. S. Berndl, E. M. Strohm, and M. C. Kolios, "High-frequency acoustic impedance imaging of cancer cells," Ultrasound Med. Biol. **41**, 2700–2713 (2015).
[89]K. Kobayashi, S. Yoshida, Y. Saijo, and N. Hozumi, "Acoustic impedance microscopy for biological tissue characterization," in *Ultrasonics* (Elsevier, 2014), Vol. 54, pp. 1922–1928.
[90]R. Fuentes-Domínguez, S. Naznin, L. Marques, F. Pérez-Cota, R. J. Smith, and M. Clark, "Characterising the size and shape of metallic nano-structures by their acoustic vibrations," Nanoscale **12**, 14230 (2020).
[91]R. McIntosh, D. Nicastro, and D. Mastronarde, "New views of cells in 3D: An introduction to electron tomography," Trends Cell Biol. **15**, 43–51 (2005).
[92]B. Hein, K. I. Willig, and S. W. Hell, "Stimulated emission depletion (STED) nanoscopy of a fluorescent protein-labeled organelle inside a living cell," Proc. Natl. Acad. Sci. U.S.A. **105**, 14271–6 (2008).
[93]M. J. Rust, M. Bates, and X. Zhuang, "Sub-diffraction-limit imaging by stochastic optical reconstruction microscopy (STORM)," Nat. Methods **3**, 793–5 (2006).
[94]N. Lassau, T. Estienne, P. de Vomecourt, M. Azoulay, J. Cagnol, G. Garcia, M. Majer, E. Jehanno, R. Renard-Penna, C. Balleyguier, F. Bidault, C. Caramella, T. Jacques, F. Dubrulle, J. Behr, N. Poussange, J. Bocquet, S. Montagne, F. Cornelis, M. Faruch, B. Bresson, S. Brunelle, A. Jalaguier-Coudray, N. Amoretti, A. Blum, A. Paisant, V. Herreros, O. Rouviere, S. Si-Mohamed, L. Di Marco, O. Hauger, M. Garetier, F. Pigneur, A. Bergère, C. Cyteval, L. Fournier, C. Malhaire, J. L. Drape, E. Poncelet, C. Bordonne, H. Cauliez, J. F. Budzik, M. Boisserie, T. Willaume, S. Molière, N. Peyron Faure, S. Caius Giurca, V. Juhan, T. Caramella, A. Perrey, F. Desmots, M. Faivre-Pierre, M. Abitbol, R. Lotte, D. Istrati, D. Guenoun, A. Luciani, M. Zins, J. F. Meder, and A. Cotten, "Five simultaneous artificial intelligence data challenges on ultrasound, CT, and MRI," Diagn. Interv. Imaging **100**, 199–209 (2019).
[95]G.-G. Wu, L.-Q. Zhou, J.-W. Xu, J.-Y. Wang, Q. Wei, Y.-B. Deng, X.-W. Cui, and C. F. Dietrich, "Artificial intelligence in breast ultrasound," World J. Radiol. **11**, 19–26 (2019).
[96]Z. Akkus, J. Cai, A. Boonrod, A. Zeinoddini, A. D. Weston, K. A. Philbrick, and B. J. Erickson, "A survey of deep-learning applications in ultrasound: Artificial intelligence–powered ultrasound for improving clinical workflow," J. Am. Coll. Radiol. **16**, 1318–1328 (2019).